Frequency-domain theory of high-order above-threshold ionization based on nonperturbative quantum electrodynamics

Bingbing Wang,[1] Lianghui Gao,[1] Xiaofeng Li,[1] Dong-Sheng Guo,[2] and Panming Fu[1,*]
[1]*Laboratory of Optical Physics, Beijing National Laboratory for Condensed Matter Physics, Institute of Physics, Chinese Academy of Sciences, Beijing 100080, China*
[2]*Department of Physics, Southern University, Baton Rouge, Louisiana 70813, USA*
(Received 10 October 2006; revised manuscript received 25 April 2007; published 25 June 2007)

High-order above-threshold ionization (ATI) is investigated in the frequency domain, based on a nonperturbative quantum electrodynamics theoretical approach. The transition matrix element of high-order ATI is expressed as a superposition of products of generalized Bessel functions, which represent probability amplitudes of finding electrons with given energies. From the frequency-domain viewpoint the high-order ATI can be described simply as an ATI followed by laser-assisted collision (LAC), and the features of high-order ATI reflect mainly the characteristics of LAC. We investigate thoroughly the LAC, finding that the plateau can be simulated by a simple classical model. We also discuss the correspondence between the time- and frequency-domain pictures of rescattering ATI.

DOI: 10.1103/PhysRevA.75.063419 PACS number(s): 32.80.Rm, 42.50.Hz, 32.80.Fb

I. INTRODUCTION

The above-threshold ionization (ATI), where an atom absorbs more photons than the minimum number necessary for ionization, is probably the most fundamental strong-field phenomenon. Since its first experiment [1] there has been considerable progress in understanding this process. Especially, the recent observations of high-order ATI [2–4] have attracted much attention. It is due to the rescattering of the ionized electron at the atomic core and shows new features, such as the appearance of a plateau with a cutoff around $10U_p$ and the sidelobes in the angular distribution of the ATI spectra. Here, U_p denotes the ponderomotive energy in the laser field.

Presently, there are two different principal approaches to the theoretical treatment of the ATI process. The first group is based on a numerical integration of the time-dependent Schrödinger equation [5]. This approach is rather complicated, and requires a large amount of computation time. The second group is based on the Keldysh-Faisal-Reiss (KFR) model [6], or the conventional strong-field approximation [7–9]. The approach generally applies the saddle-point method, and the results can be formulated in terms of the quantum-mechanical path integral, which can be related further to the three-step simple-man model [10].

The three-step model considers the temporal evolution of an electronic wave packet under the interaction of a time-dependent classical field. It can be regarded as the time-domain description of ATI. In this paper, we shall develop a frequency-domain theory of high-order ATI, based on a nonperturbative quantum electrodynamics (QED) theoretical approach. In contrast with the time-domain description of ATI, frequency-domain theory describes rescattering ATI from the viewpoint of transitions between time-independent states. Specifically, rescattering ATI consists of two steps. The first step involves the transition from the atomic ground state to a quantized-field Volkov state with momentum $\mathbf{p}_1$. This is just the direct ATI. The second step is the process of laser-assisted collision (LAC) [11–13], which involves transition from a quantized-field Volkov state with momentum $\mathbf{p}_1$ to other Volkov state with momentum $\mathbf{p}$. Importantly, each stage of the process is physical (i.e., no off-energy-shell entities appear) and can be described by a simple analytical expression. Step-by-step energy conservation is achieved in all subprocesses. We note that previously a frequency-domain theory of high-order harmonic generation (HHG) has been developed by Fu and co-workers [14–16].

The time- and frequency-domain theories of rescattering ATI provide complementary viewpoints for understanding rescattering ATI. In the frequency-domain theory the rescattering ATI can be decoupled into a direct ATI and LAC; thus, the role of these subprocesses can be investigated separately. We find that the plateau and sidelobes in the rescattering ATI spectra have their origins in LAC. By contrast, the time-domain theory analyzes the temporal evolution of the electronic wave packet in the time-dependent classical field and has the advantage of explaining the cutoff law.

This paper is organized as follows. Section 2 presents a frequency-theory of high-order ATI, where the rescattering ATI is described as an ATI followed by LAC. The transition matrix element of high-order ATI is represented by an analytic closed form. In Sec. III we establish the correspondence between the frequency- and time-domain theories of high-order ATI. We shall show that the time-dependent formula based on solving the time-dependent Schrödinger equation with a classical field can be derived from our theory. Section IV presents numerical results. Interpretation of the frequency-domain picture of rescattering ATI is given in Sec. V. Through understanding the physics underlying the generalized Bessel functions, a simple approximation for the transition matrix element of rescattering ATI is provided. Because the spectrum of the rescattering ATI reflects mainly the characteristics of LAC, it is important to understand LAC thoroughly. Section VI is devoted to this topic. The LAC exhibits similar plateaus and anomalous angular photoelec-

*Author to whom correspondence should be addressed.

tron distributions as those in the rescattering ATI. Moreover, the plateau can be simulated by a simple classical model. Finally, Sec. VII is the discussion and conclusion.

II. BASIC THEORY

We consider a quantized single-mode laser field of frequency ω. The Hamiltonian of the atom-radiation system is

$$H = H_0 + U(\mathbf{r}) + V, \tag{1}$$

where

$$H_0 = \frac{(-i\nabla)^2}{2m_e} + \omega N_a \tag{2}$$

is the free-electron and free-photon energy operator. $N_a = (a^\dagger a + aa^\dagger)/2$ is the photon number operator with a ($a^\dagger$) the annihilation (creation) operator of the laser photon mode. $U(\mathbf{r})$ is the atomic binding potential. The electron-photon interaction is

$$V = -\frac{e}{m_e}\mathbf{A}(\mathbf{r})\cdot(-i\nabla) + \frac{e^2\mathbf{A}^2(\mathbf{r})}{2m_e}, \tag{3}$$

where the vector potential is $\mathbf{A}(\mathbf{r}) = g(\hat{\boldsymbol{\epsilon}} a e^{i\mathbf{k}\cdot\mathbf{r}} + \text{c.c})$, $g = (2\omega V_e)^{-1/2}$, V_e is the normalization volume of the field, while $\hat{\boldsymbol{\epsilon}} = \mathbf{x}\cos(\xi/2) + i\mathbf{y}\sin(\xi/2)$ is the polarization vector of the laser photon mode.

The initial state of ATI is $|\psi_i\rangle = |\Phi_i(\mathbf{r}), n_i\rangle = \Phi_i(\mathbf{r}) \otimes |n_i\rangle$, which is the eigenstate of the Hamiltonian $H_0 + U(\mathbf{r})$ with energies $E_i = -E_B + (n_i + \frac{1}{2})\omega$. Here, $\Phi_i(\mathbf{r})$ is the ground-state wave function of the atomic electron with binding energy E_B, and $|n_i\rangle$ is the Fock state of the laser mode with photon number n_i. On the other hand, the final state $|\psi_f\rangle = |\Psi_{\mathbf{p}n}\rangle$ of energy $E_f = E_{\mathbf{p}n}$ is the quantized-field Volkov state [17]

$$\Psi_{\mathbf{p}n} = V_e^{-1/2} \sum_{j=-n}^{\infty} \exp\{i[\mathbf{p} + (u_p - j)\mathbf{k}]\cdot\mathbf{r}\} \mathcal{J}_j(\zeta, \eta, \phi_\xi)^* \times \exp(-ij\phi_\xi)|n + j\rangle, \tag{4}$$

which is the eigenstate of the electron–laser-mode subsystem with Hamiltonian $H_0 + V$. This eigenstate is valid under the large-photon-number approximation and its corresponding eigenvalue is $E_{\mathbf{p}n} = (\mathbf{p}^2/2m_e) + (n + \frac{1}{2} + u_p)\omega$, where $u_p = e^2\Lambda^2/m_e\omega$ is the ponderomotive energy in units of the photon energy of the laser. Further, we have $\Lambda = g\sqrt{n}$, which gives the half amplitude of the classical field in the limits $g \to 0$ and $n \to \infty$. The generalized Bessel functions $\mathcal{J}_j$ are defined in terms of ordinary Bessel functions as

$$\mathcal{J}_j(\zeta, \eta, \phi_\xi) = \sum_{m=-\infty}^{\infty} J_{-j-2m}(\zeta) J_m(\eta) e^{2im\phi_\xi}, \tag{5}$$

where $\zeta = (2|e|\Lambda/m_e\omega)\mathbf{p}\cdot\hat{\boldsymbol{\epsilon}}$, $\eta = (u_p/2)\cos\xi$, and $\phi_\xi = \tan^{-1}[(p_y/p_x)\tan(\xi/2)]$.

The time-independent feature of the fully quantized Hamiltonian enables us to treat ATI as a genuine scattering process in an isolated system that consists of the photons and the atom. Energy is conserved throughout the interaction, and formal scattering theory [18] thus applies. The boundary conditions are that U is on and V is off in the remote past, whereas V is on and U is off after collision. The corresponding scattering wave functions of the initial and final states are thus

$$\psi_i^+ = \psi_i + \frac{1}{E_i - H + i\epsilon} V\psi_i \tag{6}$$

and

$$\psi_f^- = \psi_f + \frac{1}{E_f - H - i\epsilon} U\psi_f, \tag{7}$$

respectively. Physically, ψ_i^+ is the state at $t=0$ which develops from a precollision state ψ_i in the remote past, while ψ_f^- is the state at $t=0$ which evolves to a postcollision state ψ_f in the remote future. Therefore, the S matrix for the transition from ψ_i to ψ_f is given by $S_{fi} = \langle\psi_f^-|\psi_i^+\rangle$, which can be expressed as

$$S_{fi} = \delta_{fi} - 2\pi i\delta(E_f - E_i)T_{fi}. \tag{8}$$

Here,

$$T_{fi} = \langle\psi_f^-|V|\psi_i\rangle = \langle\psi_f|V|\psi_i\rangle + \langle\psi_f|U\frac{1}{E_f - H + i\epsilon}V|\psi_i\rangle \tag{9}$$

is the transition matrix element.

The first and second terms in Eq. (9) correspond to the processes of direct and rescattering ATI. Thus, T_{fi} can be expressed as $T_{fi} = T_d + T_r$, where T_d and T_r are the transition matrix elements for the direct and rescattering ATI, respectively. In the following, we shall assume that the laser field is linearly polarized along the $\mathbf{x}$ axis; therefore $\phi_\xi = 0$ and the generalized Bessel functions become real. We also impose the long-wavelength approximation. In this case, the transition matrix element of the direct ATI becomes

$$T_d = \langle\Psi_{\mathbf{p}n}|V|\Phi_i, n_i\rangle = V_e^{-1/2}\omega(u_p - j)\Phi(\mathbf{p})\mathcal{J}_j(\zeta, \eta), \tag{10}$$

with $j = n_i - n$. Here, $\Phi(\mathbf{p})$ is the Fourier transform of the initial wave function $\Phi_i(\mathbf{r})$. On the other hand, the transition matrix element of rescattering ATI is given by

$$T_r = \langle\psi_f|U\frac{1}{E_f - H + i\epsilon}V|\psi_i\rangle = \sum_{\mathbf{p}_1 n_1}\langle\Psi_{\mathbf{p}n}|U\frac{1}{E_f - H_0 - U - V + i\epsilon}|\Psi_{\mathbf{p}_1 n_1}\rangle\langle\Psi_{\mathbf{p}_1 n_1}|V|\Phi_i, n_i\rangle. \tag{11}$$

Here, the completeness relation of the Volkov states $|\Psi_{\mathbf{p}_1 n_1}\rangle$ has been used. We assume that the effect of the binding potential U can be neglected when the electron is in the continuum; then we obtain

$$T_r = -i\pi\sum_{\mathbf{p}_1 n_1}\langle\Psi_{\mathbf{p}n}|U|\Psi_{\mathbf{p}_1 n_1}\rangle\langle\Psi_{\mathbf{p}_1 n_1}|V|\Phi_i, n_i\rangle\delta(E_f - E_{\mathbf{p}_1 n_1}). \tag{12}$$

In deriving Eq. (12) the relation $\lim_{\epsilon\to 0^+}\epsilon/[(E_f - E_\mu)^2 + \epsilon^2] = \pi\delta(E_f - E_\mu)$ has been used. The physics underlying Eq. (12)

is clear. Specifically, $\langle \Psi_{\mathbf{p}_1 n_1}|V|\Phi_i,n_i\rangle$ represents the direct ATI amplitude, where the ground-state electron absorbs $j_1=n_i-n_1$ photons from the laser field and ionizes; whereas $\langle \Psi_{\mathbf{p}n}|U|\Psi_{\mathbf{p}_1 n_1}\rangle$ represents the amplitude of LAC in which the ionized electron absorbs n_1-n photons from the field during its collision with the nucleus, and the canonical momentum of the electron changes from $\mathbf{p}_1$ to $\mathbf{p}$ as a result. Therefore, from the frequency-domain viewpoint, the rescattering ATI can be described simply as an ATI followed by LAC with all ATI channels summed up coherently. We note that the energy is conserved during these processes.

The transition matrix element of LAC can be evaluated by using the quantized Volkov states, and we obtain

$$T_{\mathrm{LAC}}=\langle \Psi_{\mathbf{p}n}|U|\Psi_{\mathbf{p}_1 n_1}\rangle = V_e^{-1}\sum_j \mathcal{J}_{j-s}(\zeta_1,\eta)\mathcal{J}_j(\zeta,\eta)\langle \mathbf{p}|U|\mathbf{p}_1\rangle, \tag{13}$$

where $s=n_1-n$ and

$$\langle \mathbf{p}|U|\mathbf{p}_1\rangle = \int d\mathbf{r}^3 \exp[-i(\mathbf{p}-\mathbf{p}_1)\cdot\mathbf{r}]U(\mathbf{r}). \tag{14}$$

By inserting Eqs. (10) and (13) into Eq. (12) we obtain the transition matrix element of the rescattering ATI of the qth order $(q=n_i-n)$

$$T_r^{(q)} = i\pi V_e^{-3/2}\sum_{\mathbf{p}_1,j_1,j}\omega(u_p-j_1)\Phi(\mathbf{p}_1)\langle \mathbf{p}|U|\mathbf{p}_1\rangle\mathcal{J}_{j_1}(\zeta_1,\eta) \times \mathcal{J}_{j_1+j-q}(\zeta_1,\eta)\mathcal{J}_j(\zeta,\eta)\delta(E_{\mathbf{p}n}-E_{\mathbf{p}_1 n_1}). \tag{15}$$

Moreover, by using the addition theorem of generalized Bessel functions

$$\sum_j \mathcal{J}_{j-s}(\zeta_1,\eta)\mathcal{J}_j(\zeta,\eta)=J_s(\zeta_1-\zeta), \tag{16}$$

we finally obtain

$$T_r^{(q)} = i\pi V_e^{-3/2}\sum_{\mathbf{p}_1,j_1}\omega(u_p-j_1)\Phi(\mathbf{p}_1)\langle \mathbf{p}|U|\mathbf{p}_1\rangle\mathcal{J}_{j_1}(\zeta_1,\eta) \times J_{q-j_1}(\zeta_1-\zeta)\delta(E_{\mathbf{p}n}-E_{\mathbf{p}_1 n_1}). \tag{17}$$

III. CORRESPONDENCE BETWEEN FREQUENCY-DOMAIN AND TIME-DOMAIN THEORIES OF HIGH-ORDER ATI

We have developed a frequency-domain theory of high-order ATI based on the formal scattering approach, which is applicable because the total Hamiltonian of the atom-radiation system is time independent due to the quantization of the field. One may ask how this approach is related to the more conventional S-matrix method based on solving the time-dependent Schrödinger equation with a classical field. Generally speaking, the connection between the formal scattering theory and the time-dependent S-matrix presentations has been discussed by Gell-Mann and Goldberger [18] and by Lippmann and Schwinger [19]. In this section, we shall show explicitly that the time-dependent formula of high-order ATI can be derived directly from our theory.

Let us start with Eqs. (8) and (9). By using the following two identities:

$$\delta(E_f-E_i)=\frac{1}{2\pi}\int_{-\infty}^{\infty}dt\exp[-i(E_i-E_f)t], \tag{18}$$

and

$$\frac{1}{E_f-H+i\epsilon}=-i\int_{-\infty}^{t}dt'\exp[-i(E_i-H+i\epsilon)(t'-t)], \tag{19}$$

because $E_f=E_i$, the rescattering part of the S matrix becomes

$$S_{fi}^r=\int_{-\infty}^{\infty}dt\,e^{-i(E_i-E_f)t}\int_{-\infty}^{t}dt'\langle\psi_f|Ue^{-i(E_i-H+i\epsilon)(t'-t)}V|\psi_i\rangle. \tag{20}$$

We make the approximation of neglecting the effect of the binding potential U when the electron is in the continuum; then we obtain

$$S_{fi}^r=\sum_{\mathbf{p}_1 n_1}\int_{-\infty}^{\infty}dt\int_{-\infty}^{t}dt'\langle\Psi_{\mathbf{p}n}|U|\Psi_{\mathbf{p}_1 n_1}\rangle e^{i(E_{\mathbf{p}n}-E_{\mathbf{p}_1 n_1})t} \times\langle\Psi_{\mathbf{p}_1 n_1}|V|\Phi_i,n_i\rangle e^{i(E_{\mathbf{p}_1 n_1}-E_i)t'}. \tag{21}$$

Now, we define a unitary operator $u(t)=\exp(i\omega t N_a)$ and rewrite Eq. (21) as

$$S_{fi}^r=\sum_{\mathbf{p}_1 n_1}\int_{-\infty}^{\infty}dt\langle\Psi_{\mathbf{p}n}|u^\dagger(t)Uu(t)|\Psi_{\mathbf{p}_1 n_1}\rangle e^{i(E_{\mathbf{p}n}-E_{\mathbf{p}_1 n_1})t} \times\int_{-\infty}^{t}dt'\langle\Psi_{\mathbf{p}_1 n_1}|u^\dagger(t') \times[u(t')Vu^\dagger(t')]u(t')|\Phi_i,n_i\rangle e^{i(E_{\mathbf{p}_1 n_1}-E_i)t'}. \tag{22}$$

Here, the unitary transforms are given by

$$u(t)|\Psi_{\mathbf{p}n}\rangle = V_e^{-1/2}e^{iE_{\mathbf{p}n}t}e^{-i[(\mathbf{p}^2/2m_e+u_p\omega)t-\mathbf{p}\cdot\mathbf{r}]} \times\sum_{j=-n}^{\infty}\mathcal{J}_j(\zeta,\eta)e^{ij\omega t}|n+j\rangle \tag{23}$$

and

$$V(t')=u(t')Vu^\dagger(t')=-\frac{e}{m_e}\mathbf{A}(t)\cdot(-i\nabla)+\frac{e^2\mathbf{A}^2(t)}{2m_e}, \tag{24}$$

where $\mathbf{A}(t)=g[\hat{\boldsymbol{\epsilon}}a\exp(-i\omega t)+\mathrm{c.c.}]$ is the time-dependent vector potential. If we neglect the difference between Fock states $|n\rangle$ of different n and replace $|n+j\rangle$ by $|n_i-1\rangle$ $(|n_i+1\rangle)$ in evaluating the matrix elements $\langle n+j|a|n_i\rangle$ $(\langle n+j|a^\dagger|n_i\rangle)$, then Eq. (22) becomes

$$S_{fi}^{r} = \int_{-\infty}^{\infty} dt \int d\mathbf{p}_1 \langle \Psi_{\mathbf{p}}(\mathbf{r},t)|U(\mathbf{r})|\Psi_{\mathbf{p}_1}(\mathbf{r},t)\rangle \times \int_{-\infty}^{t} dt' \langle \Psi_{\mathbf{p}_1}(\mathbf{r},t')|V_c(t')|\Psi_i(\mathbf{r},t')\rangle. \quad (25)$$

Here,

$$V_c(t) = -\frac{e}{m_e}\mathbf{A}_c(t)\cdot(-i\nabla) + \frac{e^2\mathbf{A}_c^2(t)}{2m_e} \quad (26)$$

is the interaction between an electron and a classical field with potential $\mathbf{A}_c(t)=\Lambda[\mathbf{x}\exp(-i\omega t)+\text{c.c.}]$, $\Psi_i(\mathbf{r},t) = e^{iE_B t}\Phi_i(\mathbf{r})$ is the time-dependent atomic ground-state wave function, and $\Psi_{\mathbf{p}}(\mathbf{r},t)$ is the classical Volkov state defined as

$$\Psi_{\mathbf{p}}(\mathbf{r},t) = V_e^{-1/2}\exp\left[i\mathbf{p}\cdot\mathbf{r} - i\frac{p^2}{2m_e}t - i\int_{-\infty}^{t} dt'\left(-\frac{e}{m_e}\mathbf{A}_c(t')\cdot\mathbf{p} + \frac{e^2\mathbf{A}_c^2(t')}{2m_e}\right)\right]. \quad (27)$$

Using a similar approach, it can be proven easily that the S matrix of direct ATI is

$$S_{fi}^{d} = -i\int_{-\infty}^{\infty} dt\langle \Psi_{\mathbf{p}}(\mathbf{r},t)|V_c(t)|\Psi_i(\mathbf{r},t)\rangle. \quad (28)$$

Equations (25) and (28) are the starting point of the strong-field approximation based on classical electromagnetic field. Most theories then applied the saddle-point method, where the high-order ATI can be formulated in terms of quantum paths, which describe the orbits of a released electron driven by the incident laser field. This approach presents the quantum-mechanical representation of the three-step simple-man model.

IV. NUMERICAL RESULTS

In the nonperturbative QED theory, the transition matrix element of high-order ATI is represented by an analytical expression in a closed and compact form. In the following, we shall present numerical results of the high-order ATI spectra and photoelectron angular distributions by using Eqs. (10) and (17). Let us consider a hydrogenlike atom (E_B =13.6 eV) irradiated by a linearly polarized neodymium-doped yttrium aluminum garnet (Nd:YAG) laser (ω =1.165 eV) of intensity 2.2×10^{14} W/cm^2. The corresponding parameters are u_p=20 and E_B/ω=11.7. The ground-state s wave function in the momentum space is assumed to have the Gaussian form $\Phi(\mathbf{p})=(4\pi/\alpha)^{3/4}\exp[-(p^2/2\alpha)]$ with α $=2m_eE_B$; while, instead of using the Coulomb potential, here a short-range atomic potential is used, i.e., $U=-\exp(-r)/r$, so that $\langle\mathbf{p}|U|\mathbf{p}_1\rangle=4\pi/[1+(\mathbf{p}-\mathbf{p}_1)^2]$.

We first consider the rescattering ATI. According to Eq. (12), the transition matrix element of rescattering ATI can be represented as the coherent superposition of LAC amplitudes, with incident electrons originating from different ATI channels. Specifically, we express Eq. (12) as $T_r=\Sigma_k T_{rk}$. Here,

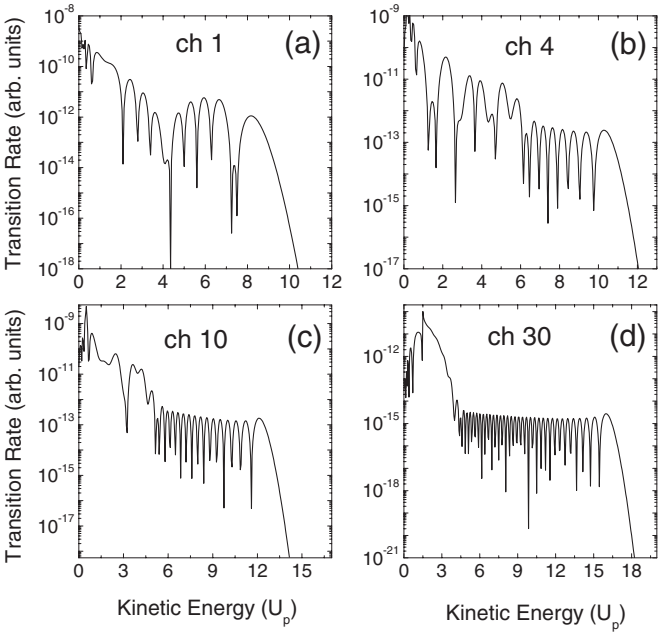

FIG. 1. Rescattering ATI of separate ATI channels for k=(a) 1, (b) 4, (c) 10, and (d) 30 when the scattered electrons are along the direction of incident field polarization. The corresponding parameters are u_p=20 and E_B/ω=11.7.

$$T_{rk} = -i\pi\sum_{\mathbf{p}_1}\langle\Psi_{\mathbf{p}n}|U|\Psi_{\mathbf{p}_1 n_1}\rangle\langle\Psi_{\mathbf{p}_1 n_1}|V|\Phi_i,n_i\rangle\delta(E_f - E_{\mathbf{p}_1 n_1}) \quad (29)$$

with $n_1=n_i-j_0-k+1$; j_0 is the minimum number of photons the atoms need to absorb to achieve ionization and k is the ordinal number of ATI channels. Figure 1 presents the rescattering ATI spectra of separate ATI channels for k=(a) 1, (b) 4, (c) 10, and (d) 30 when the scattered electrons are along the direction of the incident field polarization. We then present the rescattering ATI spectrum when contributions from all ATI channels are added up coherently (solid curve in Fig. 2). For comparison, we also present spectra with a finite number of ATI channels. The dashed, dotted, dot-dashed, and dot-dot-dashed curves in Fig. 2 present the spectra when we include one (k=1), four (k=1–4), ten (k=1–10), and 50 (k=1–50) ATI channels, respectively. These curves indicate that only four ATI channels are required to characterize the rescattering ATI spectrum with the correct cutoff. However, to obtain a good convergence at the cutoff region, as many as about 50 ATI channels should be added up coherently.

Now, we study the angular dependence of high-order ATI, which includes both direct and rescattering ATI. Let θ be the angle of the photoelectron emission with respect to the direction of incident field polarization. Figure 3 presents the ATI spectra for θ=0° (solid curve), 20° (dashed curve), and 30° (dotted curve). For θ=0°, the height of the ATI spectrum decreases generally for the kinetic energy E_k less than $2U_p$, which is then followed by a plateau with a cutoff around $10U_p$. As is well known, the low-energy region $0-2U_p$ origi-

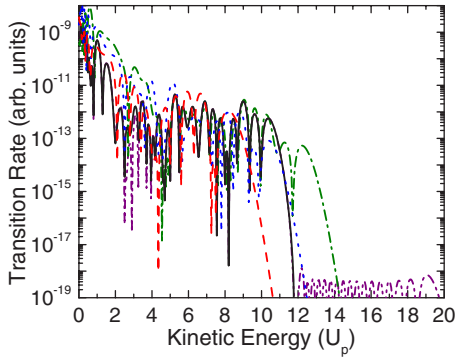

FIG. 2. (Color online) Rescattering ATI spectrum when contributions from all ATI channels are added up coherently (solid curve). For comparison, spectra that include one (dashed curve), four (dotted curve), ten (dot-dashed curve), and 50 (dot-dot-dashed curve) ATI channels are also presented. Parameters $u_p=20$ and $E_B/\omega=11.7$.

nates from the direct ionization process. On the other hand, within the high-energy plateau region $2U_p-10U_p$ the photoelectron spectrum consists almost entirely of the contribution from rescattered electrons. We also find that the cutoff energy decreases with increase of the angle of the electron emission θ.

High-order ATI is also characterized by anomalous photoelectron angular distributions [20]. Figure 4 presents the photoelectron angular distributions with (a) $E_k/U_p=2.5$ (solid curve) and 5 (dashed curve); (b) $E_k/U_p=7.5$ (solid curve) and 8.5 (dashed curve); (c) $E_k/U_p=9$ (solid curve) and 9.5 (dashed curve); (d) $E_k/U_p=10$ (solid curve) and 10.5 (dashed curve). Here, only the dependence on the polar angle θ between the directions of photoelectron emission and incident field polarization is shown, because the angular distributions are expected to have an azimuthal symmetry with respect to the field polarization axis. As is well known, the angular distributions of direct ATI are generally strongly aligned along the direction of incident field polarization. However, drastic changes are presented in angular distributions of rescattered photoelectrons, namely, within the plateau region the angular distributions become noticeably broader, and then gradually narrow on further increasing the

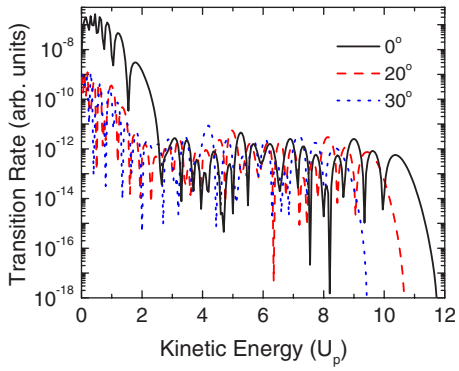

FIG. 3. (Color online) High-order ATI spectra for $\theta=0°$ (solid curve), 20° (dashed curve), and 30° (dotted curve) with parameters $u_p=20$ and $E_B/\omega=11.7$.

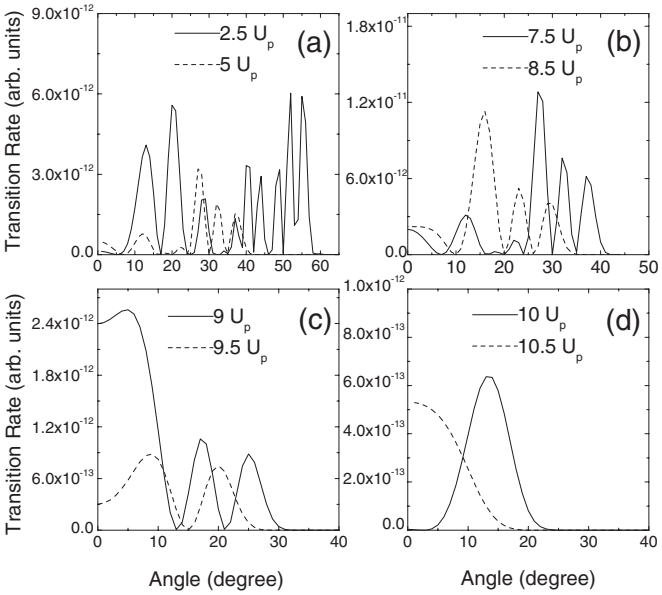

FIG. 4. Photoelectron angular distributions of high-order ATI with (a) $E_k/U_p=2.5$ (solid curve) and 5 (dashed curve); (b) $E_k/U_p=7.5$ (solid curve) and 8.5 (dashed curve); (c) $E_k/U_p=9$ (solid curve) and 9.5 (dashed curve); (d) $E_k/U_p=10$ (solid curve) and 10.5 (dashed curve). Other parameters are $u_p=20$ and $E_B/\omega=11.7$.

electron energy toward the plateau cutoff. The photoelectron angular distributions presented in Fig. 4 confirm this general rule. They also show the appearance of sidelobes in the high-energy part of the spectrum, i.e., the photoelectron emissions are concentrated mainly in a few separate narrow regions which are centered at values of the angle θ different from zero. This sidelobe structure gradually disappears near the plateau cutoff region.

V. FREQUENCY-DOMAIN INTERPRETATION OF RESCATTERING ATI

In the framework of formal scattering theory, ATI is treated as a time-independent scattering process in an isolated system that consists of photons and an atom. Thus, step-by-step energy conservation is achieved in all subprocesses, i.e., $E_i=E_{\mathbf{p}_1 n_1}=E_f$, or

$$-E_B+(n_i+1/2)\omega=(\mathbf{p}_1^2/2m_e)+(n_1+1/2+u_p)\omega$$
$$=(\mathbf{p}^2/2m_e)+(n+1/2+u_p)\omega. \quad (30)$$

Physically, Eq. (30) indicates that a ground-state atom is first ionized by absorbing $j_1=n_i-n_1$ photons from the laser field. The ionized electron then collides with the nucleus and changes its canonical momentum from $\mathbf{p}_1$ to $\mathbf{p}$ after absorbing $s=n_1-n$ additional photons. Here, although photon numbers, which approach infinity for a strong field, are involved for the requirement of energy conservation, there are just dummy parameters in our theory.

Now, let us compare the classical-field and quantized-field treatments of the motion of electrons in a laser field. For the former case, electrons exhibit quiver motion and the time-

dependent energy of electrons in a linearly polarized field is given by

$$E_c^e(t) = \frac{\mathbf{p}^2}{2m_e} + u_p\omega + \omega(\zeta \cos \omega t + 2\eta \cos 2\omega t). \quad (31)$$

Similarly, in the quantized-field theory we can eliminate the photon states and focus our attention on the electronic motion as in the case of the classical-field theory. According to Eq. (4), the quantized-field Volkov state forms a nonfactorizable entangled state of the electron and quantized field. As a consequence, although the photon number of the system is indeterminate, if we find that the field is in a state $|n-j\rangle$ with probability amplitude $\mathcal{J}_{-j}(\zeta,\eta)e^{i\mathbf{p}\cdot\mathbf{r}}$ and photon energy $(n-j+1/2)\omega$, then the energy of the electron is determined and is given by

$$E_j^e(\mathbf{p}) = E_{\mathbf{p}n} - (n-j+1/2)\omega = \frac{\mathbf{p}^2}{2m_e} + u_p\omega + j\omega. \quad (32)$$

In other words, $\mathcal{J}_{-j}(\zeta,\eta)e^{i\mathbf{p}\cdot\mathbf{r}}$ can be interpreted as the probability amplitude that an electron at $\mathbf{r}$ has energy $E_j^e(\mathbf{p})$ [16]. From this viewpoint, the motion of electrons in a quantized field has the following features. First, due to the periodic nature of the quiver motion, the electronic energy $E_j^e(\mathbf{p})$ is quantized in the quantized field. Second, a comparison between Eq. (32) and Eq. (31) indicates that $j\omega$ in Eq. (32) corresponds to the time-dependent part of the quiver motion energy, i.e., $\omega(\zeta \cos \omega t+2\eta \cos 2\omega t)$, in Eq. (31). Finally, the electronic energy $E_j^e(\mathbf{p})$ exhibits a distribution with probability amplitude given by $\mathcal{J}_{-j}(\zeta,\eta)e^{i\mathbf{p}\cdot\mathbf{r}}$. From the classical viewpoint, this corresponds to the fact that, due to the quiver motion, there are distributions of the classically laser-dressed electronic energy $E_c^e(t)$. We note that the generalized Bessel functions, which, to our knowledge, were first introduced by Brown and Kibble [21], have been widely used in multiphoton processes [22,23]. They also appear in all transition matrix elements of the multiphoton effects when they are treated by a nonperturbative QED method [14–16,24,25].

Let us consider the electronic probability amplitudes at different states during the rescattering process. First, the electron of energy $-E_B$ ionizes from the atomic ground state into the continuum through tunneling. In this process, we have, from Eqs. (30) and (32), the conservation of energy

$$-E_B = (\mathbf{p}_1^2/2m_e) + u_p\omega - j_1\omega = E_{-j_1}^e(\mathbf{p}_1). \quad (33)$$

Here, the electronic energy $E_{-j_1}^e(\mathbf{p}_1)$ is negative, manifesting the nonclassical nature of the tunneling, and the transition matrix is proportional to the probability amplitude of electrons of energy $E_{-j_1}^e(\mathbf{p}_1)$, i.e., $\mathcal{J}_{j_1}(\zeta_1,\eta)$. Subsequently, the electron has probability amplitude $\mathcal{J}_{j-s}(\zeta_1,\eta)$ of having energy $E_{s-j}^e(\mathbf{p}_1)=(\mathbf{p}_1^2/2m_e)+u_p\omega+(s-j)\omega$ before it collides with the nucleus at $\mathbf{r}=\mathbf{0}$. The electron then changes its momentum from $\mathbf{p}_1$ to $\mathbf{p}$ during the collision. Since the collision is elastic, we have $E_{s-j}^e(\mathbf{p}_1)=E_{-j}^e(\mathbf{p})$, i.e.,

$$(\mathbf{p}_1^2/2m_e) + u_p\omega + (s-j)\omega = (\mathbf{p}^2/2m_e) + u_p\omega - j\omega, \quad (34)$$

The transition matrix is proportional to $\mathcal{J}_j(\zeta,\eta)$, which is the probability amplitude of an electron having final energy $E_{-j}^e(\mathbf{p})$. Therefore, considering rescattering ATI as a direct ATI followed by LAC, the transition matrix element of the qth-order rescattering ATI is proportional to $\mathcal{J}_{j_1}(\zeta_1,\eta)\mathcal{J}_{j_1+j-q}(\zeta_1,\eta)\mathcal{J}_j(\zeta,\eta)$, as shown in Eq. (15), because the total number of photons absorbed in the rescattering ATI is $q=j_1+s$. We can make a further approximation by neglecting all details related to the atomic structure and express the transition matrix element of rescattering ATI simply as

$$T_{\mathbf{r}}^{(q)} \propto \sum_{\mathbf{p}_1,j_1,j} \mathcal{J}_{j_1}(\zeta_1,\eta)\mathcal{J}_{j_1+j-q}(\zeta_1,\eta)\mathcal{J}_j(\zeta,\eta)\delta(E_{\mathbf{p}n} - E_{\mathbf{p}_1 n_1}). \quad (35)$$

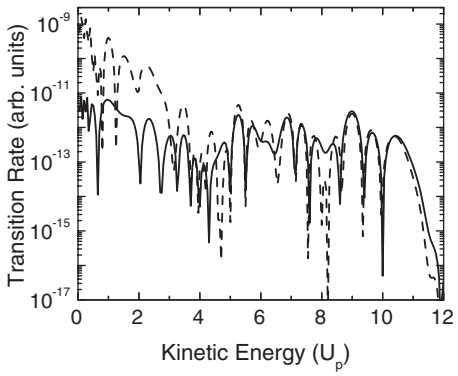

FIG. 5. Rescattering ATI spectrum based on Eq. (35), where all details related to the atomic structure are neglected (solid curve). Parameters are $u_p=20$, $E_B/\omega=11.7$, and $\theta=0°$. For comparison, the rescattering ATI spectrum based on the exact solution [i.e., Eq. (17)] is also given (dashed curve).

The solid curve in Fig. 5 presents the numerical result with parameters $u_p=20$, $E_B/\omega=11.7$, and $\phi=0°$. To check the validity of this approximation, we also plot the result based on the exact solution of the rescattering ATI (dashed curve in Fig. 5). These curves agree quite well, especially when the kinetic energy is larger than $3U_p$, indicating that the main features of the rescattering ATI originate from the interaction of the electrons with the laser field.

VI. LASER-ASSISTED COLLISION

The frequency-domain theory of high-order ATI considers the probability amplitudes of electrons at different stages, and therefore provides a different description of high-order ATI from the conventional time-domain theory. One main characteristic of this theory is that the rescattering ATI can be decoupled into a direct ATI and LAC. This decoupling enables us to investigate the physical origins of some features of rescattering ATI. In this section, we shall make detailed studies of LAC. Through comparison between the spectra of LAC and rescattering ATI, we find that the plateau and sidelobes in the rescattering ATI have their origins in LAC. The underlying physics of the plateau and angular distributions in LAC are also investigated.

We first present numerical results of LAC based on Eq. (13). The solid and dashed curves in Fig. 6 show the differ-

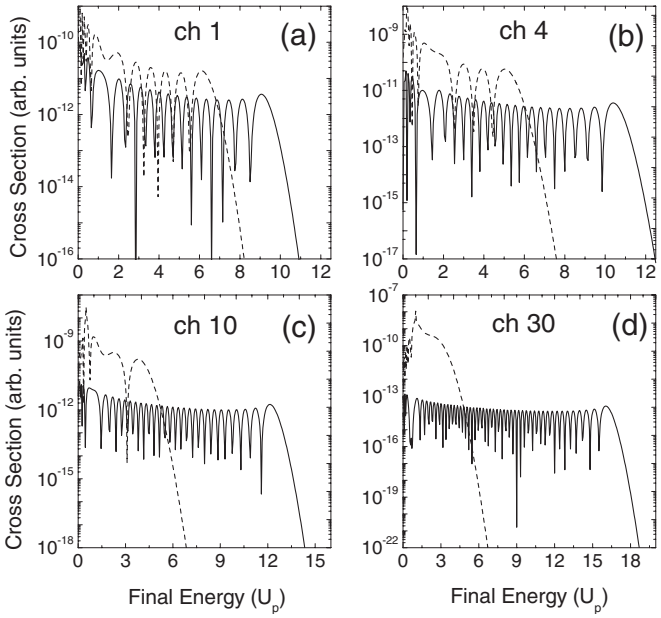

FIG. 6. Differential LAC cross sections versus the final energy for the backward (solid curve) and forward (dashed curve) scatterings when both the initial and final momenta are along the direction of incident field polarization. The incident energies are chosen to be (a) 1.55, (b) 5.05, (c) 12.04, and (d) 35.34 eV, corresponding to the first, fourth, tenth, and 30th ATI channels, respectively.

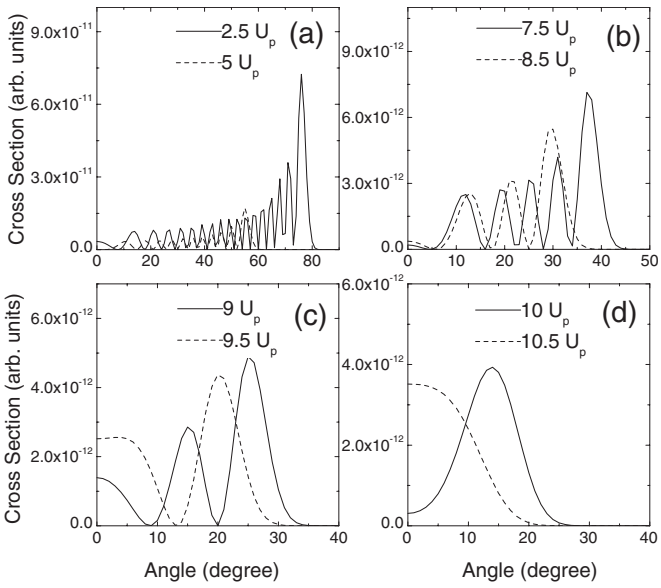

FIG. 7. Differential LAC cross sections of the backward scattering as a function of the scattering angle for (a) $E_f/U_p=2.5$ (solid curve) and 5 (dashed curve); (b) $E_f/U_p=7.5$ (solid curve) and 8.5 (dashed curve); (c) $E_f/U_p=9$ (solid curve) and 9.5 (dashed curve); (d) $E_f/U_p=10$ (solid curve) and 10.5 (dashed curve) when $E_i=5.05$ eV, corresponding to the fouth ATI channel.

ential LAC cross sections versus the final energy for the backward and forward scatterings, respectively, when both the initial and final momenta are along the direction of incident field polarization. The incident energies are chosen to be (a) 1.55, (b) 5.05, (c) 12.04, and (d) 35.34 eV, corresponding to the first, fourth, tenth, and 30th ATI channels, respectively. These spectra show plateaus with regular oscillation. Now, we turn to the rescattering ATI spectra of separate ATI channels (see Fig. 1). As is well known, the photoelectron angular distributions of the direct ATI are strongly aligned along the $\mathbf{x}$ and $-\mathbf{x}$ directions of the incident field polarization; therefore, there exist both backward and forward scatterings in the rescattering ATI. Comparing Fig. 1 with Fig. 6, we find that, when the kinetic energy E_k is larger than $E_{cutoff}^{(F)}$, which is the cutoff of the forward scattering of LAC, the rescattering ATI originates mainly from the backward scattering. By contrast, both the backward and forward scatterings contribute to the rescattering ATI when $E_k \lesssim E_{cutoff}^{(F)}$, leading to a much complicated interference structure in this regime. We then study the angular distributions of the scattered electrons. Figure 7 presents the differential LAC cross sections of the backward scattering as a function of the scattering angle for (a) $E_f/U_p=2.5$ (solid curve) and 5 (dashed curve); (b) $E_f/U_p=7.5$ (solid curve) and 8.5 (dashed curve); (c) $E_f/U_p=9$ (solid curve) and 9.5 (dashed curve); (d) $E_f/U_p=10$ (solid curve) and 10.5 (dashed curve) when $E_i=5.05$ eV, corresponding to the fourth ATI channel. Once again, we find that the angular distributions of the scattered electron show similar characteristics to those in the rescattering ATI, i.e., in the low-energy region the angular distributions are noticeably broader, and then gradually narrow on further increasing the electron energy toward the plateau cutoff. Moreover, there exist sidelobes, which gradually disappear near the plateau cutoff. One interesting thing is to compare the angular distributions of the rescattering ATI and the LAC of the fourth ATI channel, which have approximately the same cutoff. From Figs. 4 and 7, we find that they have similar angular distributions when the kinetic energy is higher than $8U_p$.

Our results demonstrate clearly that the plateau and sidelobes in the rescattering ATI have their origins in LAC. To get a better understanding of the nature of plateau and angular distribution here we analyze the electronic trajectories in LAC. Let us consider an electron in a classical field with potential $\mathbf{A}_c(t)=\Lambda[\mathbf{x}\exp(-i\omega t)+\text{c.c.}]$. The classical action, which is defined as $S_c(t,\mathbf{p})=(1/2m_e)\int dt[\mathbf{p}-e\mathbf{A}_c(t)]^2$, is

$$S_c(t,\mathbf{p})=\left(\frac{\mathbf{p}^2}{2m_e}+u_p\omega\right)t+\zeta\sin\omega t+\eta\sin 2\omega t. \quad (36)$$

Using the relation

$$\mathcal{J}_j(\zeta,\eta)=\frac{1}{2\pi}\int_{-\pi}^{\pi}d\varphi\exp[i(\zeta\sin\varphi+\eta\sin 2\varphi+j\varphi)], \quad (37)$$

we obtain

$$\mathcal{J}_j(\zeta,\eta)=\frac{\omega}{2\pi}\int_0^T dt\exp\{-i[S_c(t,\mathbf{p})-E_{-j}^e(\mathbf{p})t]\}, \quad (38)$$

where $T=2\pi/\omega$. According to Eq. (13), the transition matrix element for a scattering from an incident momentum $\mathbf{p}_i$ to a final momentum $\mathbf{p}_f$ can then be represented in terms of the classical action as

$$T_{\mathrm{LAC}} = V_e^{-1}\frac{\omega^2}{2\pi}\langle \mathbf{p}_f|U|\mathbf{p}_i\rangle \int_0^T dt\, \exp[-i\Delta S_c(t,\mathbf{p}_i,\mathbf{p}_f)], \tag{39}$$

where $\Delta S_c(t,\mathbf{p}_i,\mathbf{p}_f)=S_c(t,\mathbf{p}_i)-S_c(t,\mathbf{p}_f)$.

The time integral in Eq. (39) can be evaluated by using the saddle-point method, which gives

$$T_{\mathrm{LAC}} = V_e^{-1}\frac{\omega^2}{2\pi}\langle \mathbf{p}_f|U|\mathbf{p}_i\rangle \sum_\mu \sqrt{\frac{2\pi}{i\Delta S_c''(t_\mu,\mathbf{p}_i,\mathbf{p}_f)}} \times \exp[-i\Delta S_c(t_\mu,\mathbf{p}_i,\mathbf{p}_f)], \tag{40}$$

where the saddle points t_μ are found from

$$[\mathbf{p}_f - e\mathbf{A}_c(t_\mu)]^2 = [\mathbf{p}_i - e\mathbf{A}_c(t_\mu)]^2, \tag{41}$$

which represents an elastic scattering of electrons from an incident momentum $\mathbf{p}_i$ to a final momentum $\mathbf{p}_f$ at time t_μ. There are two real solutions of Eq. (41), corresponding to two classical trajectories, when the kinetic energy of the scattered electron is smaller than the cutoff energy. For the forward and backward scattering we have $t_1=(1/\omega)\cos^{-1}[(p_i+p_f)/4e\Lambda]$ and $(1/\omega)\cos^{-1}[(p_i-p_f)/4e\Lambda]$, respectively; while $t_2=(2\pi/\omega)-t_1$. Using these solutions, the transition matrix element can be expressed as an analytic form, given by

$$T_{\mathrm{LAC}} = \frac{\omega^2}{\pi V_e}\langle \mathbf{p}_f|U|\mathbf{p}_i\rangle \sqrt{\frac{2\pi}{\omega^2(\zeta_i-\zeta_f)\sin\omega t_1}} \times \cos[s\omega t_1 + (\zeta_i-\zeta_f)\sin\omega t_1 - \pi/4], \tag{42}$$

where $\zeta_i=(2|e|\Lambda/m_e\omega)\mathbf{p}_i\cdot\hat{\boldsymbol{\epsilon}}$ and $\zeta_f=(2|e|\Lambda/m_e\omega)\mathbf{p}_f\cdot\hat{\boldsymbol{\epsilon}}$; while $s=(\mathbf{p}_f^2-\mathbf{p}_i^2)/2m_e\omega$ is the number of photons absorbed during the collision. On the other hand, there is no classically allowed trajectory when the energy of the scattered electron is beyond the cutoff; as a result, the collision time is an imaginary value given by $t_1=(i/\omega)\cosh^{-1}[(p_f-p_i)/4e\Lambda]$.

Based on the saddle-point method, Fig. 8 presents the numerical results of LAC spectra with parameters the same as those used in Fig. 6. These results are consistent with the results using Eq. (13) (see Fig. 6). Since there are two trajectories for each classically allowed E_f, their interference gives rise to a characteristic oscillatory behavior of the LAC spectrum, which, according to Eq. (42), has minima at $s\omega t_1+(\zeta_i-\zeta_f)\sin\omega t_1-\pi/4\simeq(2n+1)\pi/2$. We then consider the angular dependence of the cutoff energy E_{cutoff} for the backward scattering. From Eq. (41), we have

$$E_{cutoff}(\phi) = \frac{1}{2}(2e\Lambda\cos\phi + \sqrt{p_i^2+4e\Lambda p_i+4e^2\Lambda^2\cos^2\phi})^2, \tag{43}$$

where the scattering angle ϕ is defined as the angle between $\mathbf{p}_f$ and $-\mathbf{x}$. This equation shows a decrease of the cutoff energy as ϕ increases, which can be explained as follows. The incident velocity of the electron at collision time t_μ equals $\mathbf{v}_i(t_\mu)=\mathbf{p}_i-e\mathbf{A}_c(t_\mu)$, while the final momentum with velocity $\mathbf{v}_f(t_\mu)$ just after the collision is given by $\mathbf{p}_f=\mathbf{v}_f(t_\mu)+e\mathbf{A}_c(t_\mu)$, where $\mathbf{v}_i(t_\mu)$ and $\mathbf{v}_f(t_\mu)$ have the same magnitude because the collision is elastic. The cutoff origins from the collision where the incident velocity has maximum magnitude $v_{max}=p_i+2|e|\Lambda$. For the backward scattering the corresponding final momentum at cutoff is $\mathbf{p}_f=-(p_i+4|e|\Lambda)\mathbf{x}$. On the other hand, if there is an angle between $\mathbf{v}_f$ and $-\mathbf{x}$ then the magnitude of $\mathbf{p}_f$ decreases as the scattering angle increases, leading to a decrease of the cutoff energy as ϕ increases. With this relationship, the broadening of the angular distribution as E_f decreases becomes evident, because the maximum scattering angle ϕ_{max} for a given final energy E_f can be estimated from $E_f\simeq E_{cutoff}(\phi_{max})$. Finally, we find that LAC spectra can be simulated by a simple classical argument. We assume that the cross section of LAC with final energy $E_f(t_\mu)$ is proportional to the time duration δt_μ where the scattered electrons have energies lying within the interval $[E_f(t_\mu),E_f(t_\mu)+\delta E_f]$. The dotted curves in Fig. 8 present our simulations of the backward scattering, where the existence of the plateau indicates that the plateau is classical in nature. The plateau can also be predicted by an analytic expression. Specifically, in the plateau regime the probability of LAC is given by

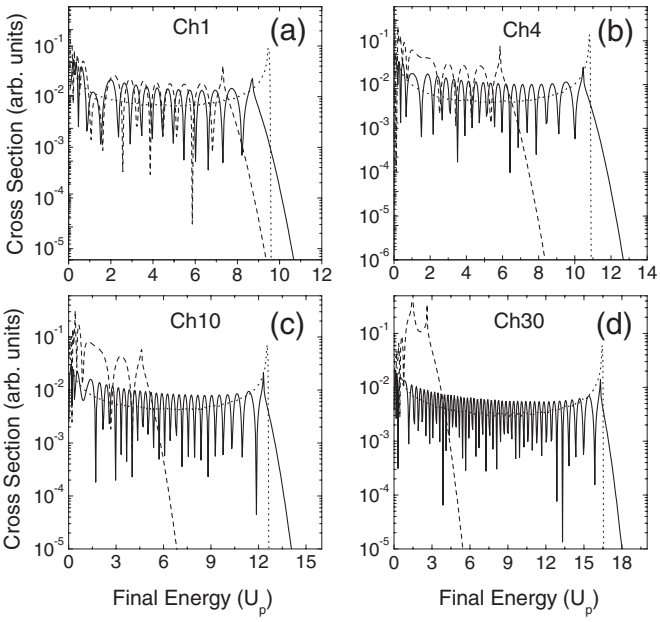

FIG. 8. Differential LAC cross sections versus the final energy for the backward (solid curve) and forward (dashed curve) scatterings calculated by the saddle-point method. Parameters are the same as those used in Fig. 6. On the other hand, the dashed curves present the results of classical simulations.

$$P \propto \delta t_\mu = \left(\frac{\partial t_\mu}{\partial E_f}\right)\delta E_f. \tag{44}$$

Since $t_\mu=(1/\omega)\cos^{-1}[(p_i-\sqrt{2m_eE_f})/4e\Lambda]$, we have

$$P \propto \frac{1}{\sqrt{2m_eE_f}\sqrt{(4e\Lambda)^2-(p_i-\sqrt{2m_eE_f})^2}}. \tag{45}$$

We note that this equation is not applicable near the cutoff because $P\to\infty$ at the cutoff.

VII. DISCUSSION AND CONCLUSION

The time- and frequency-domain theories of rescattering ATI provide complementary viewpoints for understanding rescattering ATI. For the former case, we investigate the temporal evolution of the electronic wave packet, while, for the latter case, the probability amplitudes of electrons at different stages are investigated. Let us first consider the time-domain approach to rescattering ATI, where the concept of quantum paths has proved very useful. Specifically, the matrix element of rescattering ATI can be represented as the coherent sum of exponentials of the action of these orbits [9], i.e.,

$$T_r \simeq \sum_n \left[\det\left(\frac{\partial^2 S}{\partial q_j \partial q_k} \right) \right]^{(1/2)} \exp[iS(t_n, t_n', \mathbf{p}_{1n})]. \quad (46)$$

where q_j $(j,k=1,\ldots,5)$ runs over the five variables $t, t', \mathbf{p}_1$. On the other hand, the action in Eq. (46) is

$$S(t,t',\mathbf{p}_1) = -\frac{1}{2m}\int_t^\infty d\tau[\mathbf{p} - e\mathbf{A}(\tau)]^2 - \frac{1}{2m}\int_{t'}^t d\tau[\mathbf{p}_1 - e\mathbf{A}(\tau)]^2 + \int_{-\infty}^{t'} d\tau E_B, \quad (47)$$

which illustrates the temporal evolution of the electronic wave packet: a ground state unperturbed by the field for times earlier than t', propagation in the laser field for times between the ionization time t' and the rescattering time t, and final propagation in the laser field after rescattering. The stationary points $(t_n, t_n', \mathbf{p}_{1n})$ of the action are given by the solutions of the three equations

$$[\mathbf{p}_1 - e\mathbf{A}(t')]^2 = -2mE_B, \quad (48)$$

$$[\mathbf{p}_1 - e\mathbf{A}(t)]^2 = [\mathbf{p} - e\mathbf{A}(t)]^2, \quad (49)$$

$$(t - t')\mathbf{p}_1 = \int_{t'}^t d\tau e\mathbf{A}(t). \quad (50)$$

Of these, the first expresses energy conservation when the electron at time t' tunnels into the continuum, the second enforces elastic rescattering at time t, and the third makes sure that the electron returns to its starting point.

Now, we consider the correspondence between the frequency- and time-domain pictures of rescattering ATI. Let us focus our attention on the energy of electrons at different stages in the frequency-domain approach. The energy of an electron in a quantized field is given by $E_j^e(\mathbf{p}) = (\mathbf{p}^2/2m_e) + u_p\omega + j\omega$; therefore, corresponding to Eqs. (48) and (49) we have $E_{-j_1}^e(\mathbf{p}_1) = -E_B$ and $E_{\mathbf{q}-j_1-j}^e(\mathbf{p}_1) = E_{-j}^e(\mathbf{p})$, expressing the energy conservation at the times of tunneling and elastic rescattering, respectively. Moreover, the probability amplitude of an electron having energy $E_j^e(\mathbf{p})$ is proportional to $\mathcal{J}_{-j}(\zeta,\eta)$; therefore, as a simple approximation, the matrix element of the qth-order rescattering ATI can be represented as the sum of terms $\mathcal{J}_{j_1}(\zeta_1,\eta)\mathcal{J}_{j_1+j-q}(\zeta_1,\eta)\mathcal{J}_j(\zeta,\eta)$, as presented in Eq. (35). Here, the general Bessel functions, which represent the probability amplitudes of electrons with given energies, play a similar role to the action in the time-domain theory.

Now, we discuss the underlying physics of the plateau in the rescattering ATI from the frequency-domain viewpoint. As mentioned in Ref. [16], the spectral density of the electron at the location of the nucleus after direct ATI exhibits plateaus, leading to the appearance of a plateau in the HHG. Since the kinetic energy of the electron $E_k = v^2/2m_e$, the probability of finding an electron with velocity of magnitude v also has a plateau structure. Now, according to the three-step model of rescattering ATI, there exists a correspondence between the velocities of electrons before the collision and the final energies E_f; thus, the rescattering ATI spectra exhibit plateaus also. Finally, we note that in general nonperturbative QED theory is valid for very long pulses. However, Zhang *et al.* [26] have pointed out that this approach can be adapted to the few-cycle case by treating the short pulses as a three-mode field. Using this method, they studied the carrier-envelope phase dependence of the photoelectron angular distributions in direct ATI.

In conclusion, high-order ATI is investigated in the frequency domain, based on a nonperturbative QED theoretical approach. The transition matrix element of rescattering ATI is expressed as a superposition of products of generalized Bessel functions, which represent probability amplitudes of finding electrons with given energies. From the frequency-domain viewpoint, the rescattering ATI can be described simply as an ATI followed by LAC, and the features of rescattering ATI reflect mainly the characteristics of LAC. We investigate thoroughly the LAC, finding that the plateau can be simulated by a simple classical model. We also discuss the correspondence between the time- and frequency-domain pictures of rescattering ATI.

ACKNOWLEDGMENTS

This research was supported by the National Natural Science Foundation of China under Grant No. 60478031, and the Climbing Program of the Ministry of Science and Technology of China. B.W. thanks Professor Qiren Zhu for helpful discussions.

[1] P. Agostini, F. Fabre, G. Mainfray, G. Petite, and N. K. Rahman, Phys. Rev. Lett. **42**, 1127 (1979).

[2] K. J. Schafer, B. Yang, L. F. DiMauro, and K. C. Kulander, Phys. Rev. Lett. **70**, 1599 (1993).

[3] G. G. Paulus, W. Nicklich, H. Xu, P. Lambropoulos, and H. Walther, Phys. Rev. Lett. **72**, 2851 (1994).

[4] B. Walker, B. Sheehy, K. C. Kulander, and L. F. DiMauro, Phys. Rev. Lett. **77**, 5031 (1996).

[5] E. Huens, B. Piraux, A. Bugacov, and M. Gajda, Phys. Rev. A **55**, 2132 (1997).
[6] L. W. Keldysh, Zh. Eksp. Teor. Fiz. **47**, 1945 (1964) [Sov. Phys. JETP **20**, 1307 (1965)]; F. H. M. Faisal, J. Phys. B **6**, L89 (1973); H. R. Reiss, Phys. Rev. A **22**, 1786 (1980).
[7] M. Lewenstein, K. C. Kulander, K. J. Schafer, and P. H. Bucksbaum, Phys. Rev. A **51**, 1495 (1995).
[8] A. Lohr, M. Kleber, R. Kopold, and W. Becker, Phys. Rev. A **55**, R4003 (1997); D. B. Milosevic and F. Ehlotzky, *ibid.* **58**, 3124 (1998).
[9] R. Kopold, D. B. Milosevic, and W. Becker, Phys. Rev. Lett. **84**, 3831 (2000).
[10] P. B. Corkum, Phys. Rev. Lett. **71**, 1994 (1993).
[11] N. M. Kroll and K. M. Watson, Phys. Rev. A **8**, 804 (1973).
[12] E. J. Kelsey and L. Rosenberg, Phys. Rev. A **19**, 756 (1979).
[13] L. Rosenberg and F. Zhou, Phys. Rev. A **47**, 2146 (1993).
[14] L. Gao, X. Li, P. Fu, R. R. Freeman, and D.-S. Guo, Phys. Rev. A **61**, 063407 (2000).
[15] P. Fu, B. Wang, X. Li, and L. Gao, Phys. Rev. A **64**, 063401 (2001).
[16] T. Cheng, X. Li, S. Ao, L. Wu, and P. Fu, Phys. Rev. A **68**, 033411 (2003).
[17] D.-S. Guo and T. Åberg, J. Phys. A **21**, 4577 (1988); D.-S. Guo and G. W. F. Drake, *ibid.* **25**, 3383 (1992).
[18] M. Gell-Mann and M. L. Goldberger, Phys. Rev. **91**, 398 (1953); M. L. Goldberger and K. M. Watson, *Collision Theory* (Wiley, New York, 1964).
[19] B. A. Lippmann and J. Schwinger, Phys. Rev. **79**, 469 (1950).
[20] B. Yang, K. J. Schafer, B. Walker, K. C. Kulander, P. Agostini, and L. F. DiMauro, Phys. Rev. Lett. **71**, 3770 (1993).
[21] L. S. Brown and T. W. B. Kibble, Phys. Rev. **133A**, 705 (1964).
[22] F. H. M. Faisal, *Theory of Multiphoton Processes* (Plenum, New York, 1987).
[23] A. Becker and F. H. M. Faisal, Phys. Rev. Lett. **89**, 193003 (2002).
[24] D.-S. Guo, T. Åberg, and B. Crasemann, Phys. Rev. A **40**, 4997 (1989);
[25] L. Gao, X. Li, P. Fu, and D.-S. Guo, Phys. Rev. A **58**, 3807 (1998).
[26] J. Zhang, X. Feng, Z. Xu, and D.-S. Guo, Phys. Rev. A **69**, 043409 (2004).